Optimum Geometries for Scarfed Perfect Nozzles

Jay S. Lilley*
U.S. Army Missile Command, Redstone Arsenal, Alabama 35898

The results of an investigation to determine the optimum geometry for length constrained scarfed nozzles employing perfect expansion contours is presented. A scarfed perfect nozzle performance analysis, based on an axisymmetric flowfield model and utilizing the method of characteristics solution technique, was developed. The performance model was utilized in an optimization procedure to determine, for a range of nozzle projected lengths, the optimum set of scarfed perfect nozzle geometries. For each projected length, the respective optimum nozzle geometry was selected to maximize motor axial thrust coefficient. The set of optimum scarfed nozzle geometries was compared against optimum length constrained scarfed nozzles employing conical expansion contours. The optimum scarfed perfect nozzle geometries generated by this investigation were specifically produced for utilization in a design methodology developed to minimize the length of tactical solid propellant propulsion systems. Used in conjunction with the design methodology, the results of the present investigation provide the designer with a means of further reducing propulsion system length.

Nomenclature

A = perfect nozzle contour attachment point, coefficient for optimum nozzle geometry curve-fit
B = coefficient for optimum nozzle geometry curve-fit
C = coefficient for optimum nozzle geometry curve-fit
$C_{F,x}$ = nozzle axial thrust coefficient
$C_{F,X}$ = motor axial thrust coefficient
$C_{F,y}$ = nozzle radial thrust coefficient
D = coefficient for optimum nozzle geometry curve-fit
E = scarf cut starting point, coefficient for optimum nozzle geometry curve-fit
F = cylindrical extension ending point
G = cylindrical extension starting point
H_N = nozzle projected height
L_N = nozzle projected length
$\dot{m}$ = mass flow rate
P = static pressure
P_a = ambient pressure
P_t = stagnation pressure
R^2 = curve-fit correlation coefficient
R_F = thrust coefficient ratio
R_P = pressure ratio
u = nozzle axial velocity component
X = motor axial coordinate
x = nozzle axial coordinate
X_p = nozzle projected length
Y = motor radial coordinate, curve-fit dependent variable
y = nozzle radial coordinate
Y_p = nozzle projected height
β = scarf angle
γ = specific heat ratio
ε = perfect nozzle expansion ratio
θ = cant angle
ρ_{td} = downstream throat arc radius
ρ_{tu} = upstream throat arc radius
ψ = scarf cut cross-sectional half angle

Subscripts

con = conical nozzle
e = scarf cut starting point
f = cylindrical extension ending point
g = cylindrical extension starting point
IVL = initial value line
min = minimum
per = perfect nozzle
S = scarfed
t = throat
US = unscarfed

Received June 5, 1989; revision received June 22, 1990; accepted for publication June 26, 1990. This paper is declared a work of the U.S. Government and is not subject to copyright protection in the United States.

*Aerospace Engineer, Propulsion Directorate. Member AIAA.

Introduction

In many existing and proposed tactical missile systems, the design of the guidance system requires the location of equipment (sensors, receivers, wire reels, fiber-optic bobbins) in the extreme aft section of the vehicle. Consequently, the propulsion system must be located in the midsection of the missile. In such propulsion systems, it may be necessary to employ canted nozzles that exit through the outer skin of the missile. For aerodynamic purposes, these nozzles are typically truncated, such that the exit plane of the nozzle is flush with the missile skin. Such nozzles are commonly referred to as scarfed nozzles.

The author has previously presented a procedure for optimizing the design of tactical solid propellant propulsion systems employing scarfed nozzles.[1] This procedure allows the design engineer to select the scarfed nozzle design that minimizes the overall propulsion system length. The scarfed nozzle design selection is made from a set of optimum nozzle geometries that, for a given scarfed nozzle projected length, maximize the motor axial thrust coefficient. It is evident that the principal element in the nozzle design procedure is this set of optimum nozzle geometries, and that the motor axial performance per unit length of the optimum nozzle directly influences the propulsion system length.

In the previous investigation, the nozzle geometry optimization process was restricted to scarfed nozzles with conical expansion contours. While conical nozzles offer design simplicity, there are inherent performance losses associated with their use. Specifically, there is a thrust loss resulting from flow divergence in the conical expansion contour (divergence loss).[2] Consequently, improvements in the maximum thrust coefficient for each respective projected length are possible if higher performing nonconical expansion contours are included in the scarfed nozzle optimization process. This potential improvement in performance per unit projected length would translate directly into reductions in propulsion system length. The obvious choice for a nonconical expansion contour is the perfect nozzle. The perfect nozzle is designed to produce parallel

uniform flow at a given expansion ratio and, as a result, has no divergence loss. Consequently, the implementation of perfect nozzle contours should produce the desired performance improvement.

The purpose of the present investigation is the determination of a set of optimimum scarfed nozzle geometries that employ perfect nozzle expansion contours. In conducting this investigation, a performance model for scarfed perfect nozzles was developed. The results generated by this model were incorporated in an optimization procedure used to generate a nozzle geometry set. This geometry set was compared against the optimum scarfed nozzle geometries obtained in the previous study to verify the performance advantages of employing perfect nozzle contours.

Analysis Ground Rules

The following basic ground rules were established for the analysis methods used in this investigation. These ground rules apply to all analyses performed and all results obtained in this investigation.

The following assumptions are made about the scarfed nozzle flowfield:

1) The gas is thermally and calorically perfect.

2) The presence of condensed phases and chemical reactions are neglected.

3) Boundary-layer effects are negligible.

4) The flow is irrotational (constant entropy and stagnation enthalpy).

5) The flowfield through the scarfed nozzle is axisymmetric. This assumption is valid as long as the scarf angle exceeds the local Mach angles along the scarf cut. The utilization of an axisymmetric flowfield model implies that the external nozzle flowfield does not influence performance.

6) The flowfield in the cylindrical extension is parallel and uniform, and at the same conditions as the end of the perfect contour.

These assumptions are consistent with the use of an axisymmetric method-of-characteristics (MOC) flowfield analysis model. The use of an MOC analysis is justified by the results of two previous investigations.[3,4] In these previous studies, performance predictions generated by an MOC flowfield model were compared against experimental performance data for a wide range of small scarfed nozzle geometric configurations. The close agreement between predicted and measured nozzle performance (within 10%) demonstrates the validity of using an MOC based model in the present investigation. The following general rules apply to the performance analysis of scarfed nozzles:

1) The motor axial thrust coefficient is independent of stagnation pressure, atmospheric pressure, stagnation temperature, and molecular weight.

2) The motor axial thrust coefficient is only a function of nozzle geometry and specific heat ratio.

Geometric Model

Presented in Fig. 1 is an illustration of the scarfed nozzle geometric model employed in the present investigation. The basic nozzle consists of circular arcs forming a throat section that attaches smoothly to a perfect nozzle supersonic expansion contour. The nozzle extension consists of a cylindrical section attached to the basic nozzle. The axis of the nozzle, x, is canted at an angle θ with respect to the missile axis X. The nozzle is truncated flush to the missile skin (parallel to the missile axis) by a planar scarf cut, which intersects the nozzle axis at the scarf angle β, which is equal to the cant angle θ.

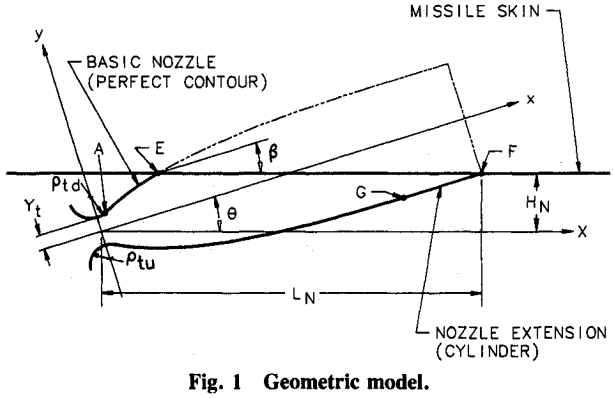

Fig. 1 Geometric model.

The basic nozzle contour is completely specified by the specific heat ratio of the gas used, γ, the throat radius y_t, the upstream arc radius ρ_{tu}, the downstream arc radius ρ_{td}, and the expansion ratio of the perfect nozzle contour, ε. The expansion ratio is given by the following expression:

$$\varepsilon = (y_g/y_t)^2 \tag{1}$$

where y_g is the nozzle contour radius at Point G. Point G denotes the end of the perfect nozzle contour and the start of the cylindrical nozzle extension. The nozzle extension is simply a cylinder of radius y_g, which is added to the perfect nozzle contour at Point G.

Two additional parameters are required to complete the specification of the nozzle geometry; the scarf angle β and the nozzle projected length L_N. The value of L_N is the projected length of the nozzle along the missile axis, X, as measured from the center of the throat. The specification of β and L_N determines the location of Point E, which is the starting point of the scarf cut, and Point F, the ending point.

The scarfed nozzles considered in the present geometric model are completely specified by the following design parameters: y_t, γ, ρ_{tu}, ρ_{td}, ε, β, and L_N. An additional dependent nozzle design parameter is the projected height H_N, which is the distance between the center of the throat and the missile skin measured perpendicular to the missile axis. For the purposes of generalizing the geometry model, the values of L_N and H_N have been nondimensionalized with respect to the throat radius. The nondimensionalized projected length X_p and height Y_p are given by

$$X_p = L_N/y_t \tag{2}$$

$$Y_p = H_N/y_t \tag{3}$$

The set of nozzle design parameters, therefore, are y_t, γ, ρ_{tu}, ρ_{td}, ε, β, and X_p.

Performance Model

The performance model employed in the present investigation is based on a computer code developed by Hoffman.[2] This code is based on an axisymmetric flowfield model, and utilizes the numerical MOC solution technique. The perfect nozzle solution technique is described in detail in Ref. 2. For a given set of nozzle design parameters (y_t, γ, ρ_{tu}, ρ_{td}, and ε), the code is used to determine the corresponding unique perfect nozzle wall contour. The code also determines the flowfield properties along that contour.

After the perfect nozzle contour has been determined, the unscarfed nozzle geometry is completed by the addition of the cylindrical extension. By definition, there is parallel and uniform flow at the end of the perfect nozzle contour (Point G), and the flow in the cylindrical extension is assumed to be parallel and uniform with the same properties.

The performance factor that is of interest in the present investigation is the thrust coefficient, as measured along the missile axis, the motor axial thrust coefficient $C_{F,X}$, which is given by the following relationship:

$$C_{F,X} = C_{F,x} \cos\theta - C_{F,y} \sin\theta \tag{4}$$

where $C_{F,x}$ is the thrust coefficient measured along the nozzle axis (x-axis), and $C_{F,y}$ is the thrust coefficient measured in the nozzle radial direction (y-axis).

The values of $C_{F,x}$ and $C_{F,y}$ are determined by numerically integrating the nozzle wall pressure over the actual scarfed nozzle wall geometry. The value of $C_{F,x}$ is given by the following relationships:

$$C_{F,x} = C_{F,x\text{IVL}} + C_{F,x\text{US}} + C_{F,xS} \tag{5}$$

where $C_{F,x\text{IVL}}$ is the nozzle axial thrust coefficient of the initial value line, which is the thrust coefficient of the throat, $C_{F,x\text{US}}$ is the nozzle axial thrust coefficient of the unscarfed nozzle section that starts at the throat and ends at Point E, and $C_{F,xS}$ is the nozzle axial thrust coefficient of the scarfed portion of the nozzle that starts at Point E and ends at Point F.

These nozzle axial thrust coefficients are given by the following relationships:

$$C_{F,x\text{IVL}} = [1/(\pi y_t^2 P_t)] \int_{\text{IVL}} (2\pi y\, P\mathrm{d}y + u\, \mathrm{d}\dot{m}) \tag{6}$$

$$C_{F,x\text{US}} = 2/y_t^2 \int_{y_t}^{y_e} (P/P_t) y\, \mathrm{d}y \tag{7}$$

$$C_{F,xS} = 2/(y_t^2\pi) \int_{y_e}^{yf} (\pi - \psi)(P/P_t) y\, \mathrm{d}y \tag{8}$$

where IVL is the surface formed by the initial value line, u is the nozzle axial component of velocity, $\dot{m}$ is the mass flow rate through the nozzle, P is the wall static pressure, and P_t is the stagnation pressure. The subscripts e and f denote the respective points on the nozzle wall, and ψ is the half-angle formed by the section of wall removed by the scarf cut at a given nozzle axial location. This angle is illustrated in Fig. 2.

The value of $C_{F,y}$ is determined by applying the following relationship to integrate the wall pressure over the scarfed portion of the nozzle (from Point E to Point F):

$$C_{F,y} = 2/(y_t^2\pi) \int_{x_e}^{xf} (P/P_t) y \sin\psi\, \mathrm{d}x \tag{9}$$

The integration procedure for the scarfed portion of the nozzle is illustrated in Fig. 2. The specific details of the performance integration process are given in Ref. 5.

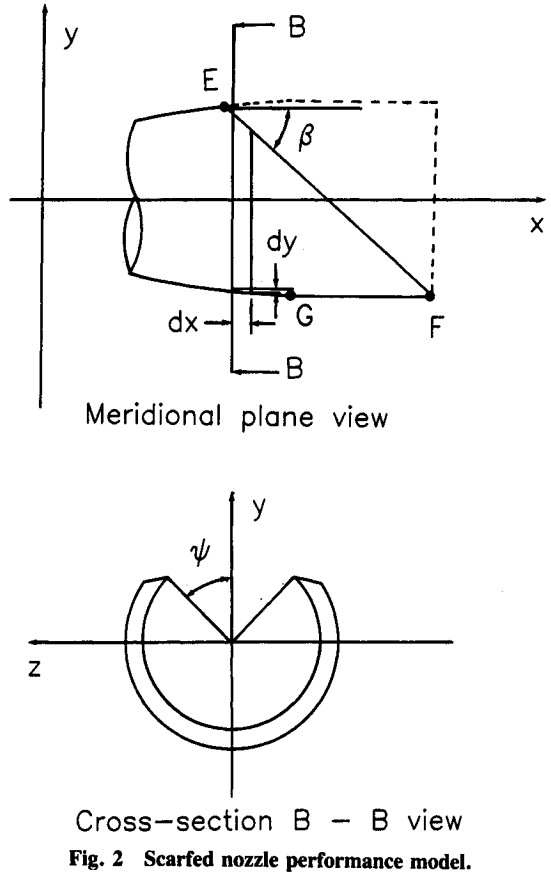

Fig. 2 Scarfed nozzle performance model.

Optimization Analysis

An optimization analysis was performed to determine the set of scarfed nozzle geometries that maximized the motor axial thrust coefficient for various nozzle projected lengths. In the optimization study, the following perfect nozzle design parameters were selected as being typical values for tactical missiles (also compatible with those used in the previous study[1]):

$$y_t = 1.0 \text{ in.}, \qquad \rho_{tu}/y_t = 1.0, \qquad \rho_{tu}/y_t = 0.5, \qquad \gamma = 1.2$$

The independent design variables utilized in the optimization study were β, ε, and Xp, and the dependent variable was $C_{F,X}$. For this study, the following ranges of independent variables were evaluated:

$$\beta_{min} < \beta < 80°, \qquad 1.5 \le \varepsilon \le 60, \qquad 5 \le X_p \le 50$$

where β_{min} is the minimum allowable scarf angle for a nozzle with fixed values of ε and X_p. When the scarf angle is equal to β_{min}, the scarf cut intersects the throat.

Applying the previously specified input parameters, the flowfield analysis code was used to determine the perfect nozzle wall contours and wall static pressure distributions for 60 different expansion ratios encompassing the required range of values (an expansion ratio of 1.5, and all integer values of ε from 2 to 60 were evaluated). A cylindrical extension of appropriate diameter and sufficient length was added to each of the 60 perfect nozzle contours.

For a given value of X_p and for a given nozzle contour, specified by ε, an optimization search was performed on β to maximize the value of $C_{F,X}$. The result of this search was an intermediate optimum value of $C_{F,X}$ (and corresponding β) for a specific X_p and ε combination. For a given X_p value, this procedure was repeated for each of the 60 ε values (perfect nozzle contours). Consequently, for each value of X_p there was a set of 60 intermediate optimum $C_{F,X}$ values that each corresponded to a particular ε value. Forty-six X_p values (evenly distributed over the specified range in increments of 1) were evaluated. For each value of X_p, an interpolation procedure was used on the intermediate optimums to determine an estimate of the value of ε that would produce the global maximum for $C_{F,X}$. Each of these 46 estimated global optimum values of ε was used to generate a corresponding unscarfed nozzle contour and pressure profile. To improve the resolution of the global optimization process, for each of these 46 contours additional intermediate optimum geometries were also determined for each X_p value. Consequently, for each X_p value, 106 intermediate optimum geometries were determined, each corresponding to a perfect nozzle contour (ε value). From each of the 46 sets of intermediate optimum geometries (which each corresponded to a given X_p value), a global optimum geometry was selected that had the maximum motor axial thrust coefficient for the given X_p value. These global optimum geometries, which are characterized by values of ε and β and a performance level of $C_{F,X}$, represent the maximum performing scarfed perfect nozzles for the respective projected lengths.

Presented in Fig. 3 is a plot of the overall nozzle optimization surface for the case of $X_p = 20$. The results in Fig. 3 are typical of those achieved for the other projected length values. In Fig. 3, the optimization process is illustrated by

consideration of a fixed value of ε. This ε value corresponds to a unique perfect nozzle contour, and is represented by a $C_{F,X}$-β plane. The curve that is projected in this plane illustrates the influence of scarf angle (cant angle) on axial performance for a given contour. Note that the projected nozzle length is fixed for all points in Fig. 3. By changing the scarf angle, the nozzle is canted to make the scarfed surface parallel to the missile axis, and the scarf cut location is adjusted to achieve the proper projected length. The β value maximizing $C_{F,X}$ corresponds to the intermediate optimum geometry. In Fig. 3, 106 such $C_{F,X}$-β planes were utilized to determine the set of intermediate optimums that is represented by the peak line on the $C_{F,X}$-β-ε surface. The maximum $C_{F,X}$ value on the intermediate optimum line corresponds to the global optimum mode geometry for the given X_p value. The intermediate optimum line and the global optimum are illustrated in Fig. 3. It is interesting to note that for all values of ε, the intermediate value of β is very close to the minimum value. (This was true for the other X_p values.) This result would indicate that the cosine term in Eq. (1) tends to dominate the optimization procedure. Consequently, reducing the scarf angle is key to maximizing performance.

Optimization Results

The optimization study produced a set of optimum length constrained scarfed perfect nozzles. The results of this optimization study are presented in Figs. 4–9. Presented in Figs. 4–8 are plots of the optimum values of ε, β, Y_p, $C_{F,X}$ and minimum pressure ratio, P_{min}/P_t, each respectively plotted as a function of X_p. In Figs. 5–8, the results that correspond to the perfect scarfed nozzles determined by the present investigation are labeled "perfect" in the plot legend. The values of P_{min}/P_t presented in Fig. 8 represent the minimum wall static pressure ratio that occurs throughout the cylindrical extension. Presented in Fig. 9 are the optimum scarfed perfect nozzle contours for X_p = 5, 10, 15, 20, 25, 30, 35, 40, 45, and 50. Presented in Table 1 are the geometric specifications of the nozzles presented in Fig. 9.

The results presented in Figs. 4–8 for the perfect scarfed nozzles were curve-fitted to the following relationships:

$$Y = AX_p^4 + BX_p^3 + CX_p^2 + DX_p + E \qquad (10)$$

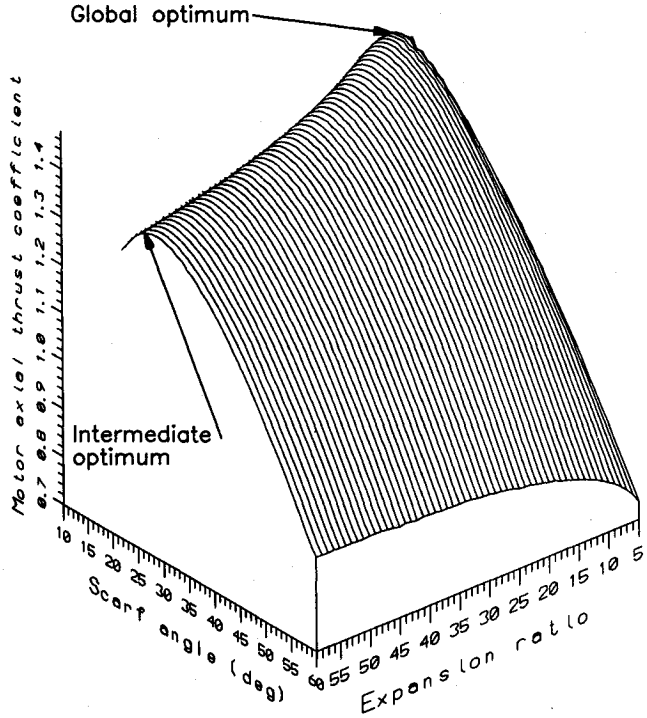

Fig. 3 Typical optimization solution surface (X_p = 20).

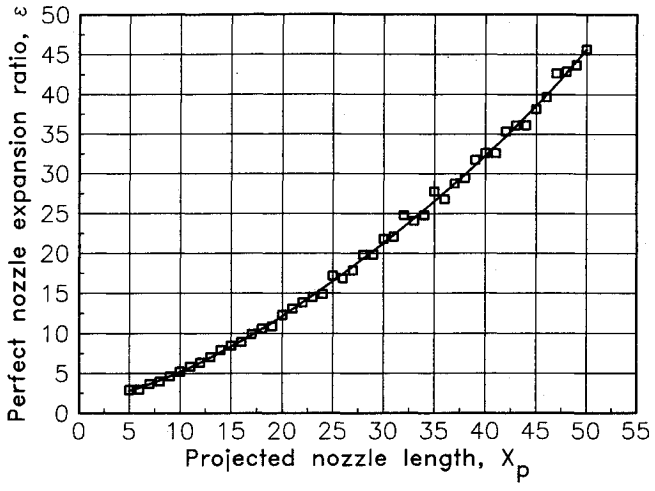

Fig. 4 Optimum perfect nozzle expansion ratio as a function of projected length.

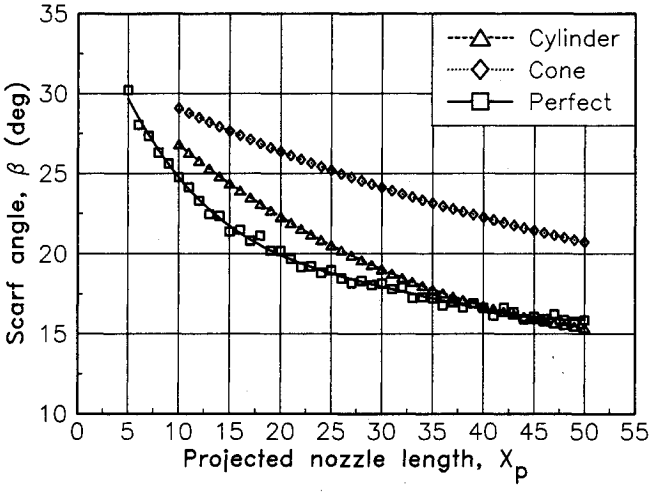

Fig. 5 Optimum scarf angle as a function of projected length.

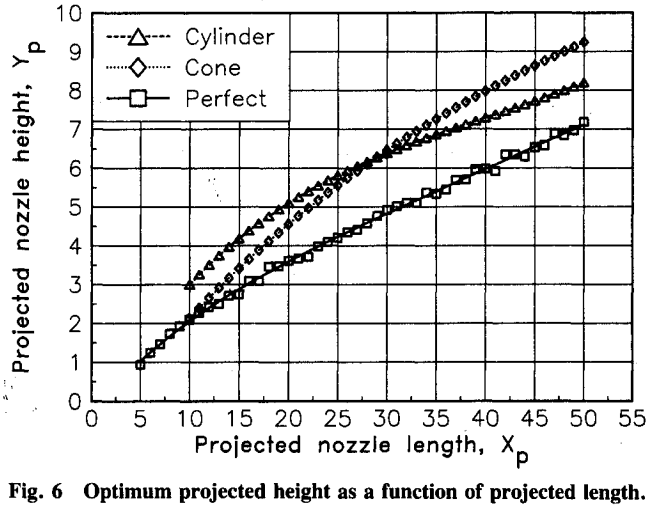

Fig. 6 Optimum projected height as a function of projected length.

where

Y is ε, β(deg), Y_p, or $C_{F,X}$

A, B, C, D, and E are curve-fit coefficients

and

$$Y = AX_p^B \qquad (11)$$

where Y is P_{min}/P_t.

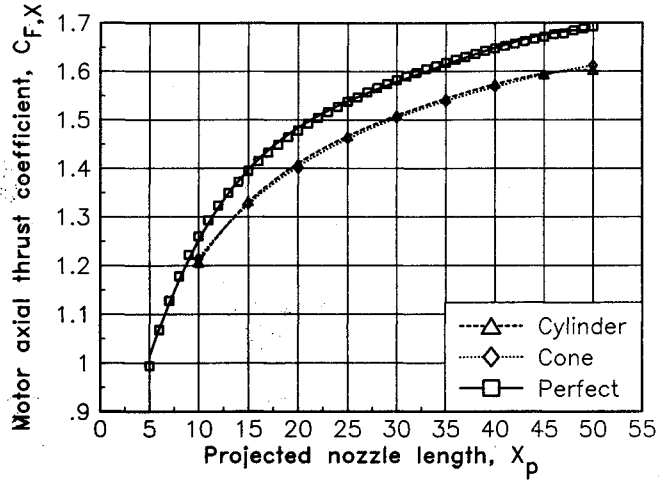

Fig. 7 Optimum motor axial thrust coefficient as a function of projected length.

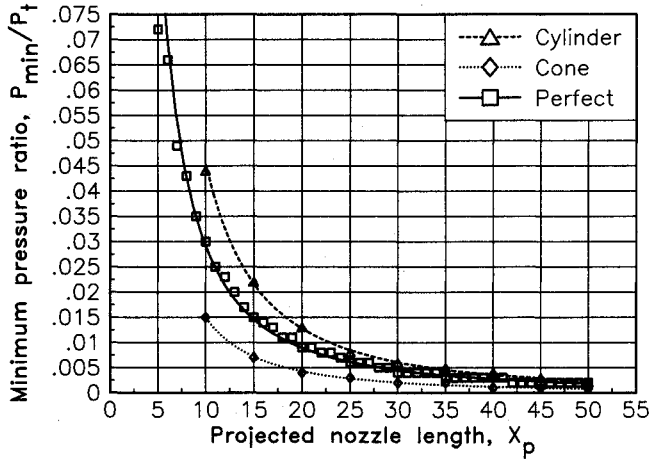

Fig. 8 Optimum minimum pressure ratio as a function of projected length.

The coefficients for each of the curve-fits, along with the correlation coefficients R^2, are presented in Table 2. For all the curve-fits, the value of R^2 exceeded 0.99, which indicates extremely good agreement between the curve-fits and the optimization results.

The relationships presented in Eqs. (10) and (11) and coefficients in Table 2 form a convenient mathematical model for the determination of the optimum perfect scarfed nozzle geometries and their corresponding performance. For a given X_p value, the optimum perfect scarfed nozzle geometry is determined by the following procedure:

1) Equation (10) is used to determine the optimum values of ε and β.

2) The computer code developed by Hoffman is used to generate the perfect nozzle contour for the optimum ε value (and the previously specified values of y_t, γ, ρ_{tu}, and ρ_{td}).

3) A cylindrical extension is added to the perfect contour.

4) The nozzle is canted at the optimum value of β.

5) The nozzle is truncated parallel to the missile skin at the correct X_p value.

By using the above procedure, optimum nozzle geometries can be generated for the complete range of X_p values considered by the study. This nozzle construction procedure, used along with the curve-fit relationships in Eqs. (10) and (11) and the corresponding coefficients in Table 2, can be directly applied to the propulsion system optimization procedure described in Ref. 1.

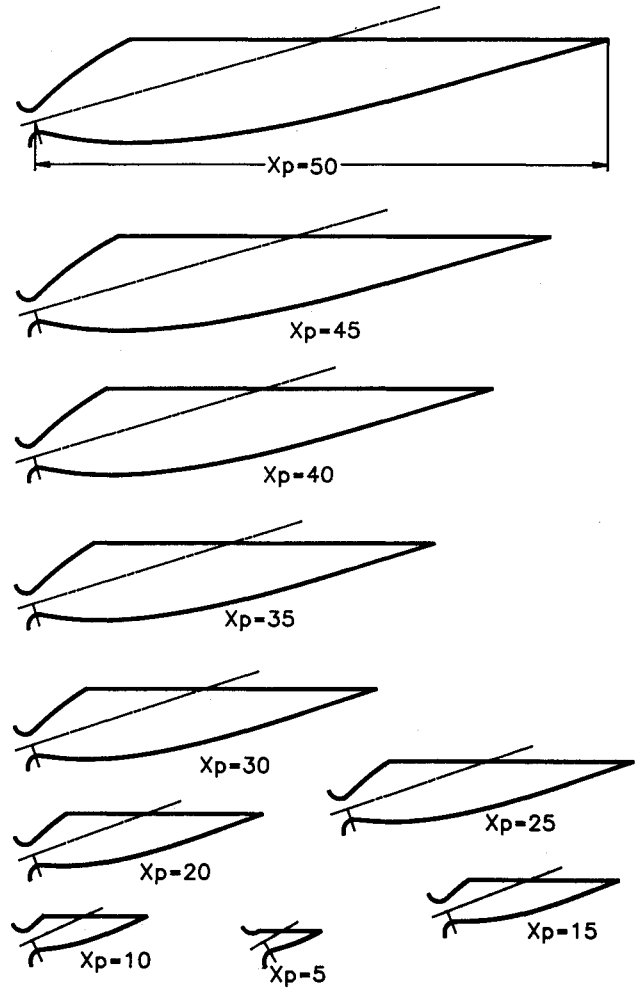

Fig. 9 Optimum nozzle configurations.

Table 1 Optimum scarfed perfect nozzle specifications

X_p	ε	β, deg	Y_p	$C_{F,X}$	P_{min}/P_t
5	2.927	30.23	0.934	0.9944	0.07207
10	5.212	24.76	2.101	1.2599	0.02976
15	8.458	21.38	2.750	1.3939	0.01549
20	12.274	20.18	3.614	1.4783	0.00946
25	17.178	18.96	4.205	1.5376	0.00611
30	21.813	18.15	4.922	1.5823	0.00449
35	27.763	17.23	5.336	1.6178	0.00329
40	32.601	16.63	5.985	1.6469	0.00268
45	38.147	16.07	6.532	1.6713	0.00219
50	45.622	15.86	7.187	1.6921	0.00175

Comparisons with Optimum Conical Nozzles

The fundamental objective of the present investigation was to determine optimum scarfed nozzle geometries that were superior to those developed in Ref. 1. Consequently, a direct comparison between the results obtained in the two investigations is required. For the purposes of comparison, the results from the previous investigation are presented in Figs. 5–8, along with the perfect nozzle results. In the previous investigation, optimization studies were conducted for two conical scarfed nozzle configurations: nozzles with cylindrical scarfed extensions, and scarfed conical nozzles with no extensions. The results from these studies are labeled "cylinder" and "cone," respectively, in Figs. 5–8.

The results in Fig. 5 indicate that, for X_p values up to 42, the scarfed perfect nozzles have a lower scarf angle than the conical designs. For X_p values between 42 and 50, the perfect nozzle has a lower scarf angle than the nozzle with no exten-

Table 2 Curve-fit coefficients

Y	A	B	C	D	E	R^2
ε	3.6249E−06	−4.1753E−04	2.6764E−02	1.3363E−01	1.5276E−00	0.99822
β, deg	1.0535E−05	−1.4393E−03	7.4439E−02	−1.8687E+00	3.7341E+01	0.99637
Y_p	−7.6095E−07	1.1612E−04	−6.6519E−03	2.8442E−01	−2.3989E−01	0.99803
$C_{F,X}$	−5.1721E−07	7.0709E−05	−3.6414E−03	9.0783E−02	6.4191E−01	0.99100
P_{min}/P_t	1.4820E+00	−1.7064E+00	—	—	—	0.99192

sion, and virtually the same scarf angle as the nozzle with the cylindrical extension. The results in Fig. 6 indicate that the perfect nozzle has a lower projected nozzle height than either conical design. This fact is a direct result of the lower (or equivalent) scarf angles, as shown in Fig. 5. The lower nozzle projected height is an attractive feature, as it makes the nozzle easier to package in a diameter limited tactical system.

The results in Fig. 7 indicate that the scarfed perfect nozzles have superior performance to either conical nozzle design. To further illustrate the performance advantage achieved with scarfed perfect nozzles, presented in Fig. 10 is a plot of the thrust coefficient ratio R_F, as a function of projected length, where

$$R_F = C_{F,X_{per}}/C_{F,X_{con}} \tag{12}$$

$C_{F,X_{per}}$ is the thrust coefficient for the optimum scarfed perfect nozzle, and $C_{F,X_{con}}$ is the thrust coefficient for the optimum scarfed conical nozzle (with or without an extension). The results presented in Fig. 10 show that the use of a scarfed perfect nozzle will result in a performance increase of 3.8% over that of both conical nozzle designs over the range of projected lengths considered. For X_p values equal to 15 or above, the performance increase is greater than 4.6%.

The results presented in Fig. 8 show that the minimum pressure ratios for the perfect nozzles are less than those for the conical nozzles with the extension but greater than those for the conical nozzles without the extension. To further illustrate this difference, presented in Fig. 11 is a plot of pressure ratio R_p, as a function of projected length where

$$P = (P_{min}/P_t)_{per}/(P_{min}/P_t)_{con} \tag{13}$$

Here, $(P_{min}/P_t)_{per}$ is the minimum pressure ratio for the optimum scarfed perfect nozzle, and $(P_{min}/P_t)_{con}$ is the minimum pressure ratio for the optimum scarfed conical nozzle (with or without an extension). The results in Fig. 11 show that the perfect nozzle has a minimum pressure ratio that is at least 25% lower than that of the conical nozzle with a cylindrical extension, and at least 103% higher than that of a conical nozzle with no extension.

In previous investigations, it has been theoretically and experimentally shown that the motor axial thrust coefficient

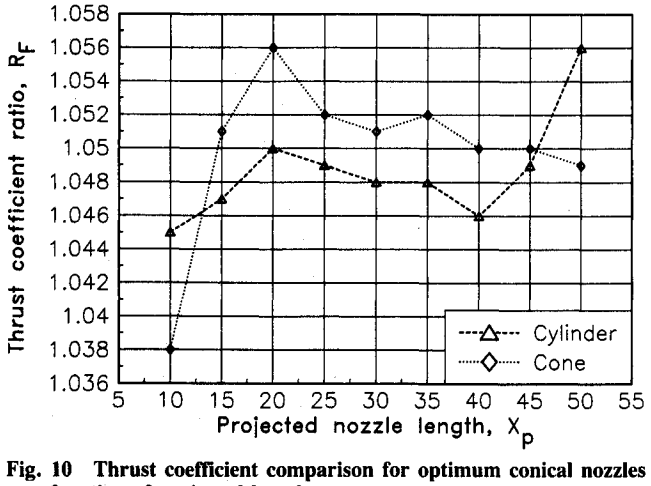

Fig. 10 Thrust coefficient comparison for optimum conical nozzles as a function of projected length.

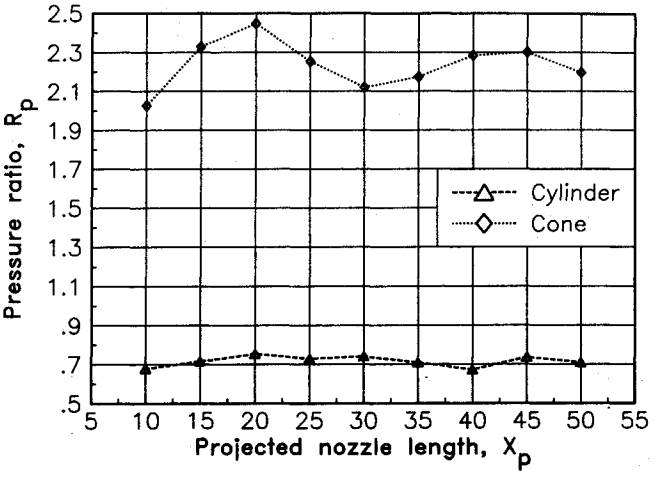

Fig. 11 Pressure ratio comparison for optimum conical nozzles as a function of projected length.

of a scarfed nozzle is independent of stagnation pressure.[3,4] However, this pressure independence is based on the assumption that the flow in the scarfed extension is not separated. If flow separation occurs, the performance levels determined in this investigation are invalidated. A previous investigation by the author experimentally demonstrated that separation in the nozzle is dependent on both the ratio of minimum pressure in the nozzle, P_{min}, to the ambient pressure P_a and the nozzle length.[4] For a fixed nozzle length, the experimental results demonstrated that the flowfield in a scarfed extension will separate when P_{min}/P_a falls below a given minimum level. This minimum P_{min}/P_a level represents a separation criteria for scarfed nozzles that can be applied to evaluate the range of operating conditions for which a given nozzle design is valid. This criteria is discussed in detail in Ref. 4. On the basis of the previous results, it can be assumed that, for a given nozzle length (or projected length), the primary determining factor for nozzle separation is the ratio of minimum pressure to ambient pressure. Thus, for a given X_p value, P_{min}/P_a is an indicator of the lowest nozzle stagnation pressure for which the predicted performance is applicable. For a fixed ambient pressure, the results presented in Fig. 11 show the relative applicability of the three optimum scarfed nozzle geometry sets. For a given X_p value, the perfect scarfed nozzle will separate at a pressure that is at least 33% higher than that of the conical nozzle with the cylindrical extension, and at least 51% lower than that of the conical nozzle with no extension. Therefore, the optimum conical nozzles with the cylindrical extensions can be utilized at lower stagnation pressures than are possible with the perfect nozzles.

The higher separation pressure of the scarfed perfect nozzle is a factor limiting propulsion system design flexibility. To reduce the separation pressure levels, off-optimimum designs were considered. Specific intermediate optimum designs were considered for each X_p value utilizing an ε value less than the optimum. This process is illustrated in Fig. 3 by consideration of points along the peak line that have $C_{F,X}$ values that are less than the global optimum. Presented in Fig. 12 is a plot of the values of R_F plotted against the values of R_p for the various intermediate optimums for the case of the conical scarfed nozzle with the cylindrical extension. Presented in Fig. 13 are corresponding values for the conical nozzle with no

extension. From the results in Fig. 12, it can be seen that, for equivalent minimum pressure ratios (R_p = 1.0), the perfect nozzle produces a performance improvement of greater than 3.8%. For X_p values equal to 15 or above, the performance improvement is greater than 4.3%. To further illustrate this result, presented in Table 3 are selected results from Fig. 12 for the case of RP = 1.0. An alternative perspective on the results in Fig. 12 shows that the use of the perfect nozzle will yield equivalent performance with at least a 44% reduction in minimum allowable stagnation pressure. In Fig. 13, it is shown that a 103% improvement in minimum pressure ratio can be achieved with a greater than 3.8% performance gain. For X_p values 15 and above, performance gain is greater than 5%. Alternatively, the results in Fig. 13 also indicate that the same performance can be achieved with at least an 80% reduction in the minimum allowable stagnation pressure. Therefore, if off-optimum designs are considered, a greater than 3.8% (greater than 4.3% for X_p values of 15 and above) performance improvement can be achieved with no degradation in minimum operating pressure. Alternatively, off-optimum perfect nozzles can be employed to reduce the minimum allowable operating pressure by at least 44%, without any loss in nozzle performance.

The results in Figs. 11, 12, and 13 require some interpretation from the standpoint of gas dynamics. The conical nozzles with scarfed extensions exhibit the highest P_{min}/P_t values for a given X_p value. This result is due to the oblique shock wave that occurs at the discontinuity between the basic nozzle and the extension. The result is an abrupt pressure rise at the discontinuity and high pressure levels throughout the extension.[5] The conical nozzle with no extension has no discontinuity and has a continuously decreasing pressure in the scarfed portion, due to the increasing wall diameter. Consequently, this type of nozzle has the lowest P_{min}/P_t values. The P_{min}/P_t level of the scarfed perfect nozzles fall between that of the other two designs. This result is due to the fact that, although there is no discontinuity to raise the pressure, there is also no expansion in the scarfed extension to reduce it. The selection of off-optimum perfect nozzle designs raises the P_{min}/P_t value by decreasing the expansion ratio (and, thus, increasing the exit pressure of the basic nozzle contour). Consequently, the performance produced by the higher expansion ratio is sacrificed to achieve higher pressures in the scarfed extension (and a greater pressure range).

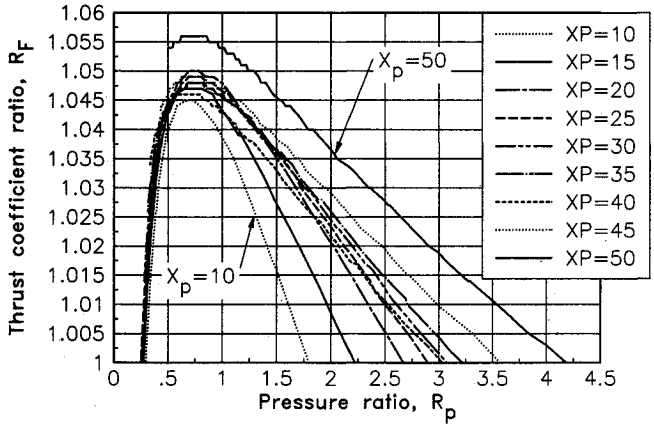

Fig. 12 Thrust coefficient ratio as a function of pressure ratio for optimum conical nozzles (cylindrical extension).

Table 3 Thrust coefficient ratios for R_p = 1.0 for optimum conical nozzles with cylindrical extensions (δ = 0°)

X_p	ε	R_F
10	3.9381	1.0385
15	6.6072	1.0435
20	9.9088	1.0476
25	13.4721	1.0467
30	17.2937	1.0458
35	21.2518	1.0458
40	23.8948	1.0430
45	30.0215	1.0468
50	34.8050	1.0540

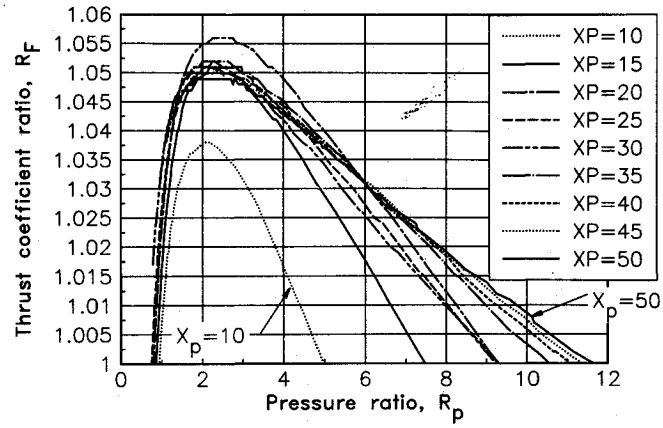

Fig. 13 Thrust coefficient ratio as a function of pressure ratio for optimum conical nozzles (conical extension).

Conclusions

A set of optimum scarfed perfect nozzle geometries have been determined, which, for given nozzle projected lengths, maximize motor axial thrust coefficient. The set of optimum scarfed perfect nozzles was compared against sets of optimum scarfed conical nozzles derived from a previous study. The perfect nozzles were shown to provide at least a 3.8% increase in motor axial performance. If off-optimum scarfed perfect nozzles were considered, at least a 3.8% increase in performance is possible, with no compromises made on motor operating pressure. Alternatively greater operating pressure flexibility could be achieved with off-optimum designs with no performance loss, as compared to the optimum conical nozzles. This optimum set of nozzle geometries was specifically intended for implementation in a previously developed propulsion system design methodology. This methodology was developed to minimize the length of tactical propulsion systems employing scarfed nozzles. The performance improvement provided by the use of the scarfed perfect nozzles translates directly into a reduction in propulsion system length, when compared to those generated using optimum scarfed conical nozzles.

Acknowledgments

The author wishes to express his appreciation to Professor Joe D. Hoffman of Purdue University for providing the perfect nozzle analysis code utilized in this investigation.

References

[1]Lilley, J. S., "The Design and Optimization of Propulsion Systems Employing Scarfed Nozzles," *Journal of Spacecraft and Rockets*, Vol. 23, No. 6, 1986, pp. 597–604.

[2]Zucrow, M. J., and Hoffman, J. D., *Gas Dynamics*, Vol. II, Wiley, NY, 1977, pp. 160–164.

[3]Lilley, J. S., and Hoffman, J. D., "Performance Analysis of Scarfed Nozzles," *Journal of Spacecraft and Rockets*, Vol. 23, No. 1, 1986, pp. 53–62.

[4]Lilley, J. S., "Experimental Validation of a Performance Model for Scarfed Nozzles," *Journal of Spacecraft and Rockets*, Vol. 24, No. 6, 1987, pp. 474–480.

[5]Hoffman, J. D., "A Computer Program for the Performance Analysis of Scarfed Nozzles," U.S. Army Missile Command, RK-CR-84-3, May 1984.